Figure S1.

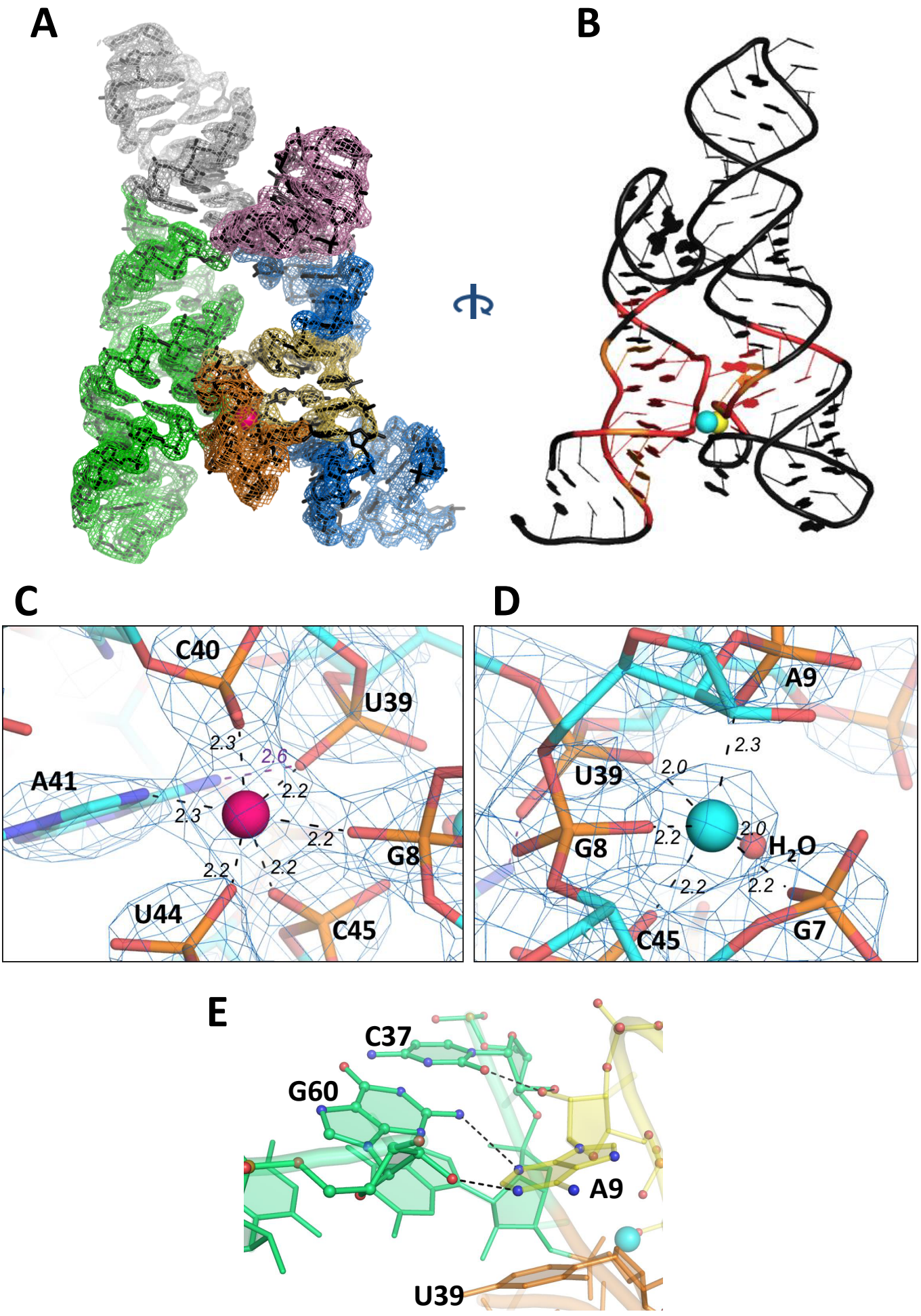
A
B
C
C40
U39
A41
G8
U44
C45
2.3
2.6
2.2
D
A9
U39
G8
C45
G7
2.0
H_2O
E
C37
G60
A9
U39

Figure S2.

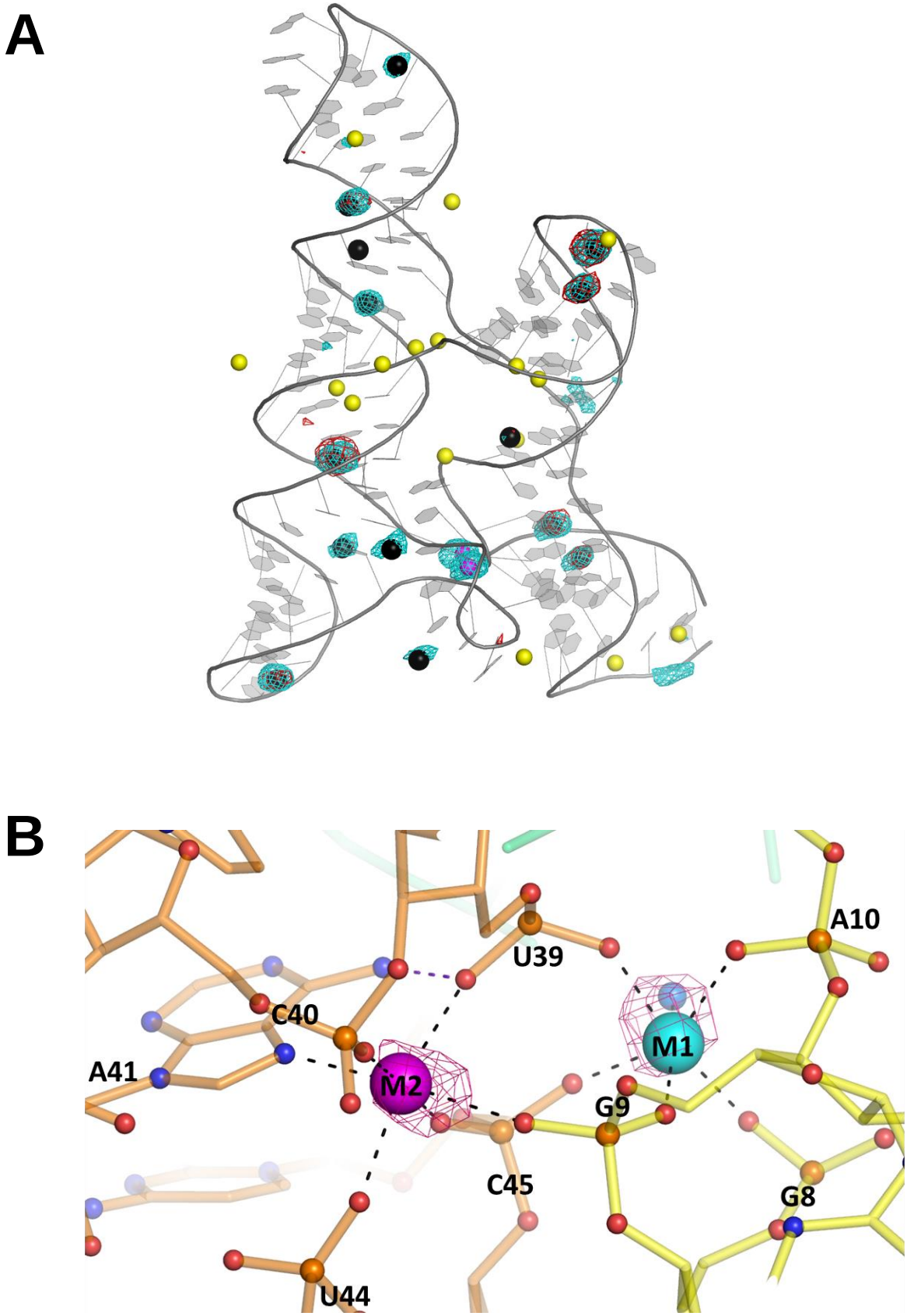

A

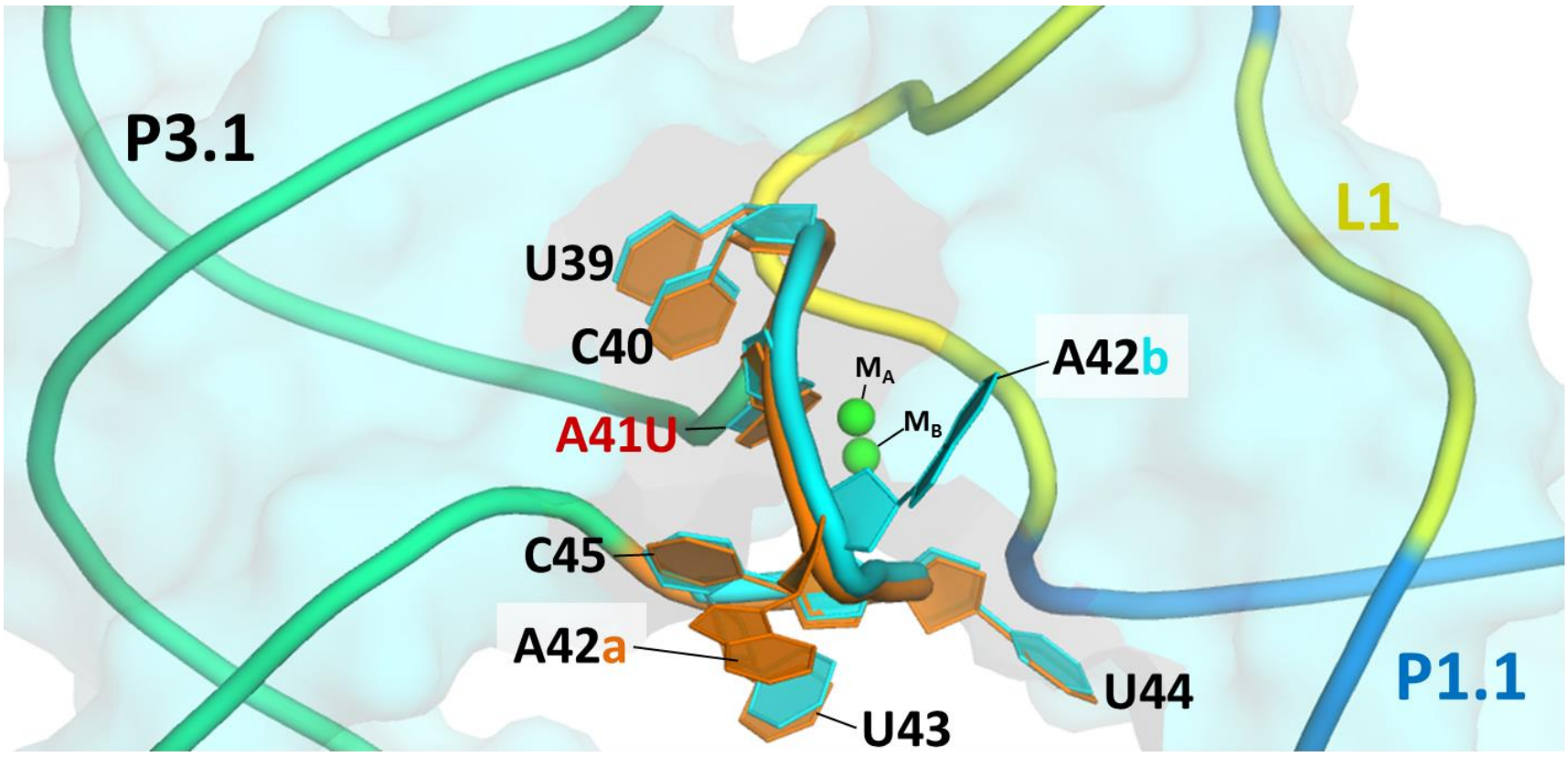
P3.1
L1
U39
C40
A41U
M_A
M_B
A42b
C45
A42a
U43
U44
P1.1

B

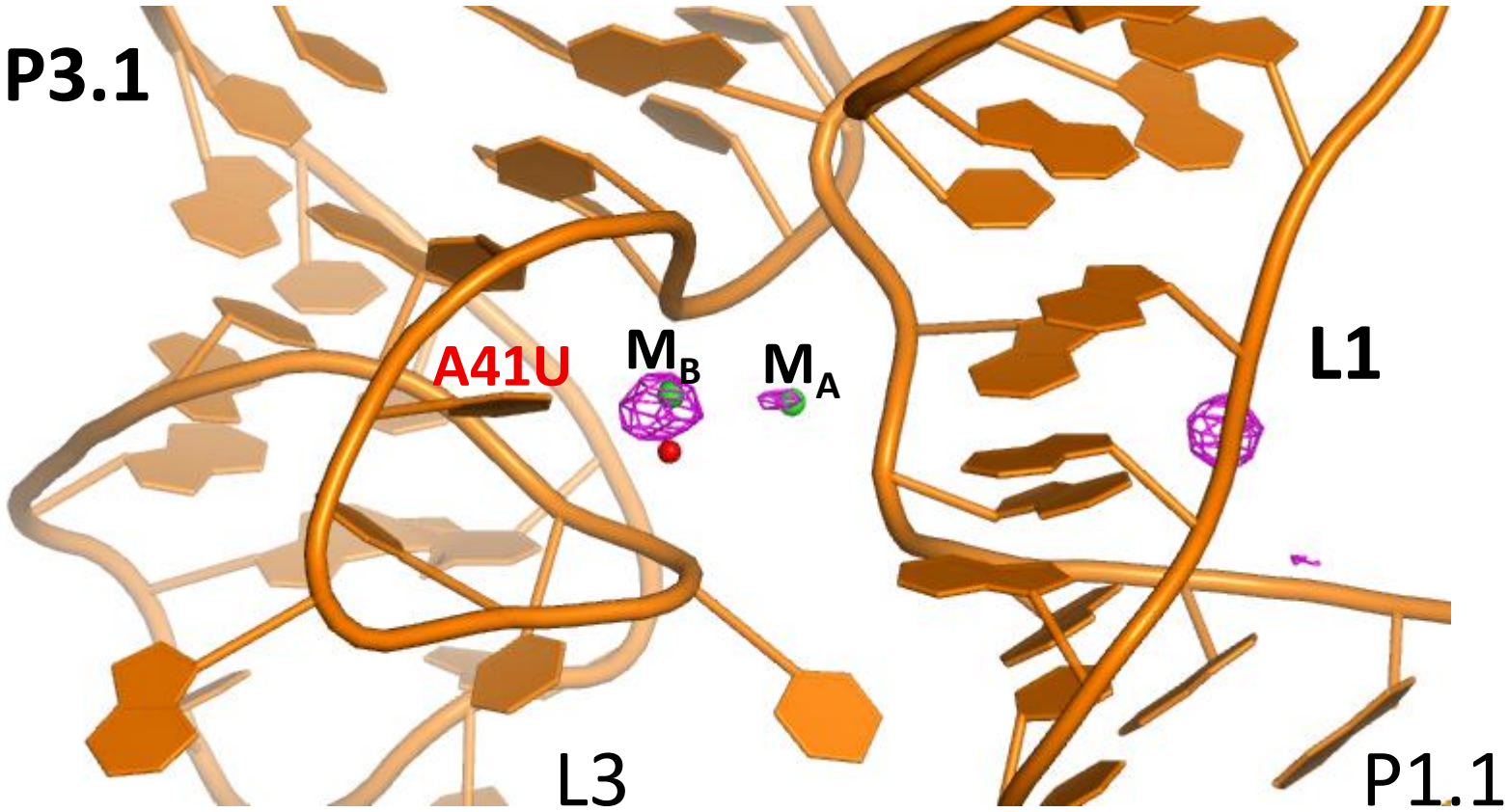
P3.1
A41U
M_B
M_A
L1
L3
P1.1

Figure S4.

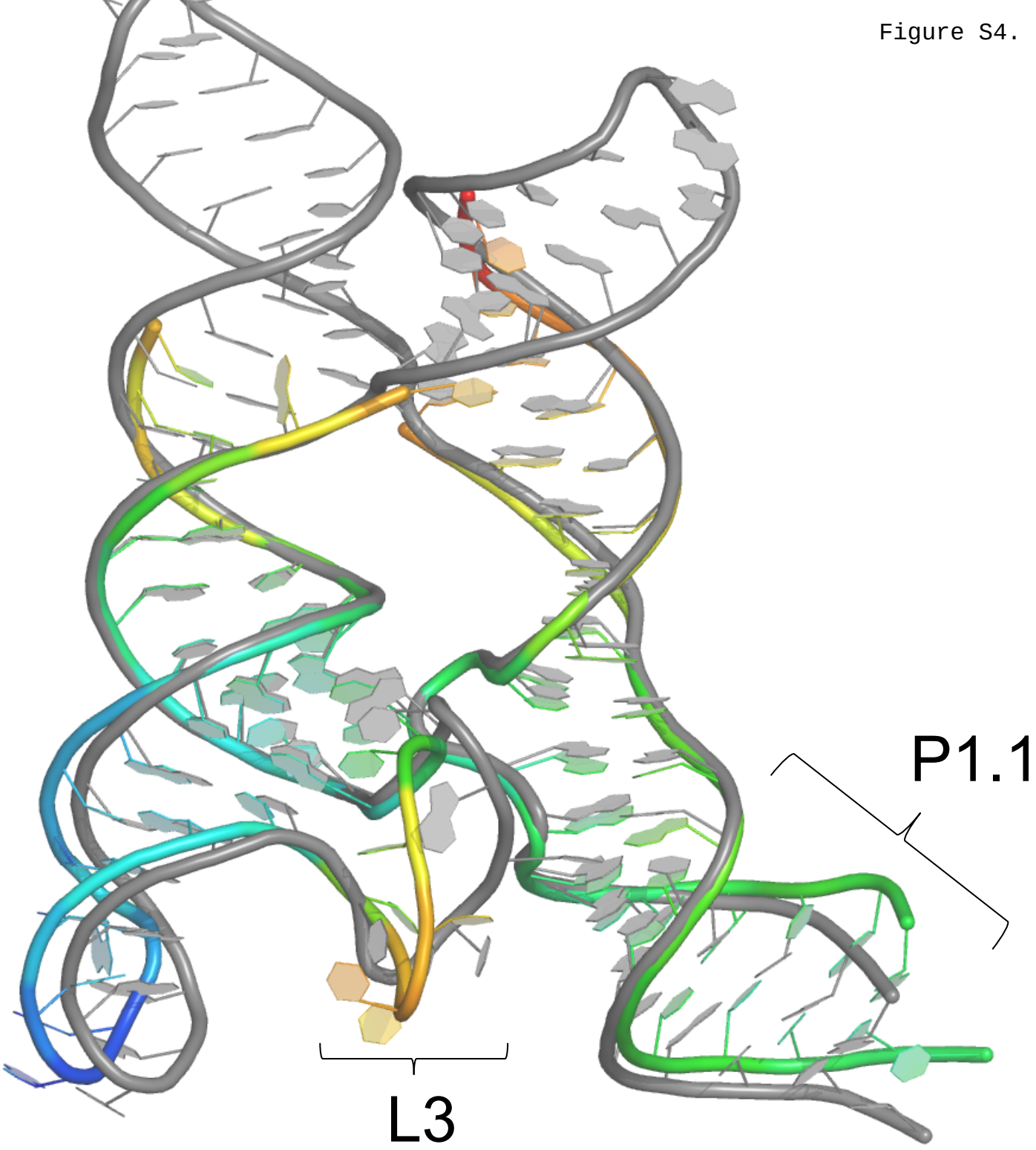

Figure S5.

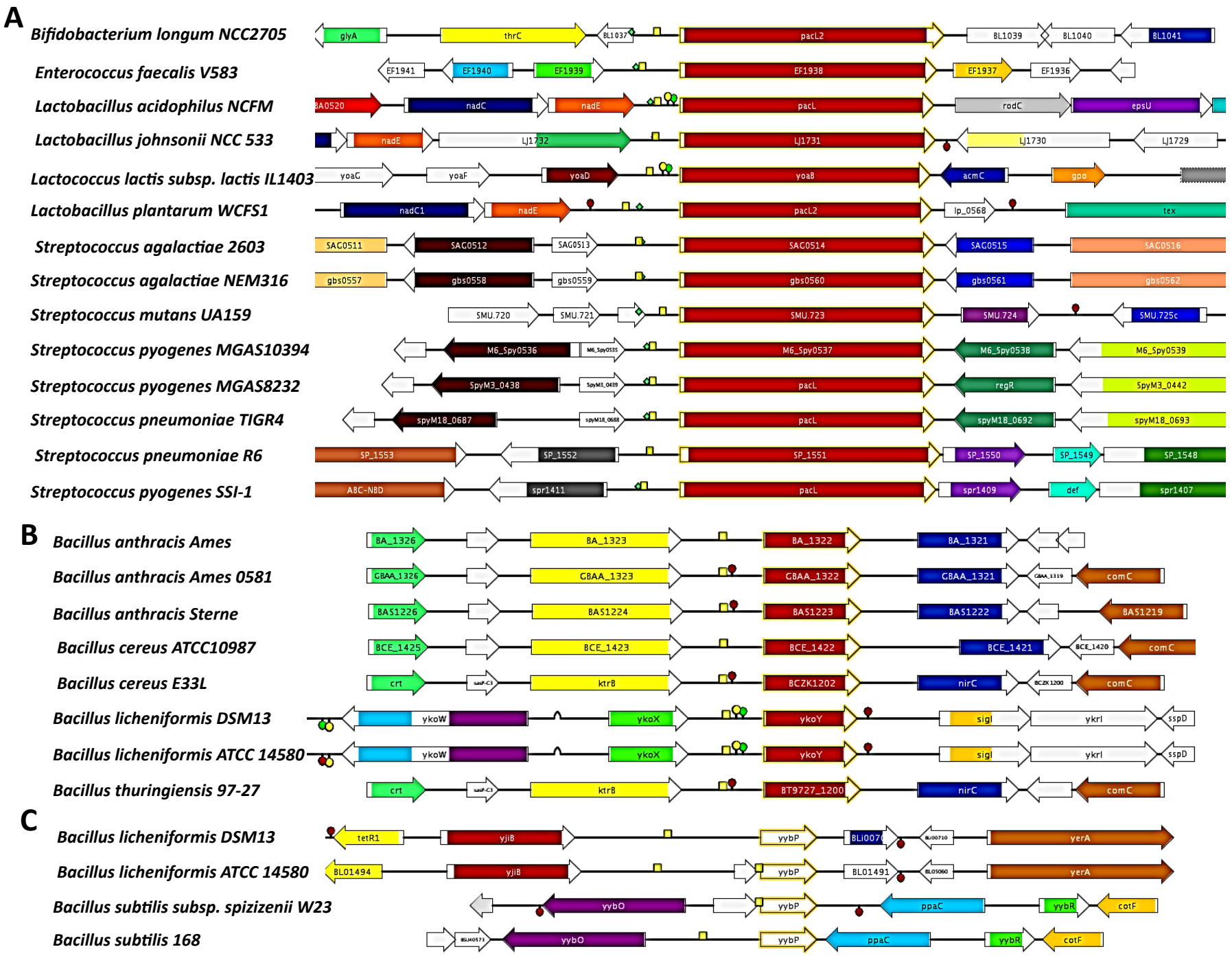
A
Bifidobacterium longum NCC2705
glyA thrC BL1037 pacL2 BL1039 BL1040 BL1041
Enterococcus faecalis V583
EF1941 EF1940 EF1939 EF1938 EF1937 EF1936
Lactobacillus acidophilus NCFM
BA0520 nadC nadE pacL rodC epsU
Lactobacillus johnsonii NCC 533
nadE LJ1732 LJ1731 LJ1730 LJ1729
Lactococcus lactis subsp. lactis IL1403
yoaG yoaF yoaD yoa8 acmC gpo
Lactobacillus plantarum WCFS1
nadC1 nadE pacL2 lp_0568 tex
Streptococcus agalactiae 2603
SAG0511 SAG0512 SAG0513 SAG0514 SAG0515 SAG0516
Streptococcus agalactiae NEM316
gbs0557 gbs0558 gbs0559 gbs0560 gbs0561 gbs0562
Streptococcus mutans UA159
SMU.720 SMU.721 SMU.723 SMU.724 SMU.725c
Streptococcus pyogenes MGAS10394
M6_Spy0536 M6_Spy0537 M6_Spy0538 M6_Spy0539
Streptococcus pyogenes MGAS8232
SpyM3_0438 pacL regR SpyM3_0442
Streptococcus pneumoniae TIGR4
spyM18_0687 pacL spyM18_0692 spyM18_0693
Streptococcus pneumoniae R6
SP_1553 SP_1552 SP_1551 SP_1550 SP_1549 SP_1548
Streptococcus pyogenes SSI-1
ABC-N8D spr1411 pacL spr1409 def spr1407
B
Bacillus anthracis Ames
BA_1326 BA_1323 BA_1322 BA_1321
Bacillus anthracis Ames 0581
GBAA_1326 GBAA_1323 GBAA_1322 GBAA_1321 comC
Bacillus anthracis Sterne
BAS1226 BAS1224 BAS1223 BAS1222 BAS1219
Bacillus cereus ATCC10987
BCE_1425 BCE_1423 BCE_1422 BCE_1421 comC
Bacillus cereus E33L
crt ktrB BCZK1202 nirC comC
Bacillus licheniformis DSM13
ykoW ykoX ykoY sigI ykrI sspD
Bacillus licheniformis ATCC 14580
ykoW ykoX ykoY sigI ykrI sspD
Bacillus thuringiensis 97-27
crt ktrB BT9727_1200 nirC comC
C
Bacillus licheniformis DSM13
tetR1 yjiB yybP yerA
Bacillus licheniformis ATCC 14580
BL01494 yjiB yybP BL01491 yerA
Bacillus subtilis subsp. spizizenii W23
yybO yybP ppaC yybR cotF
Bacillus subtilis 168
yybO yybP ppaC yybR cotF

Figure S6.

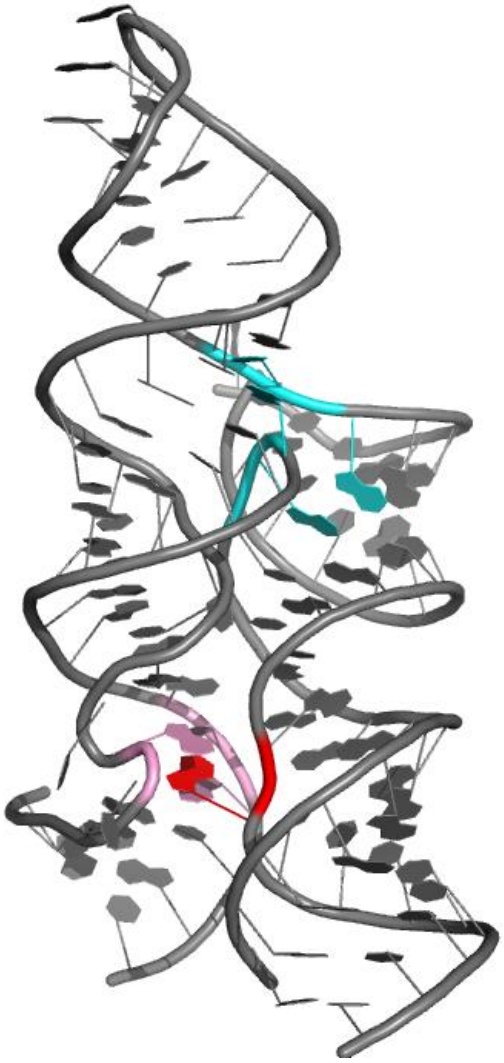

Hairpin ribozyme
PDB ID: 1M5K

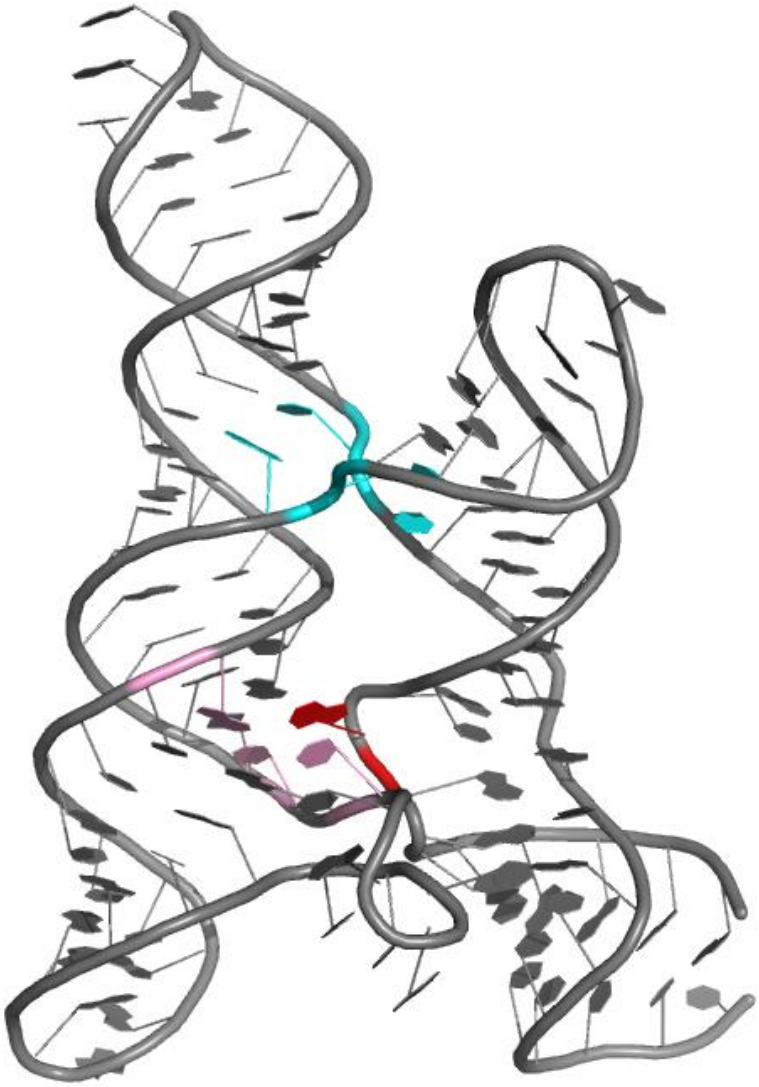

L. Lactis yybP-ykoY
riboswitch

Figure S7.

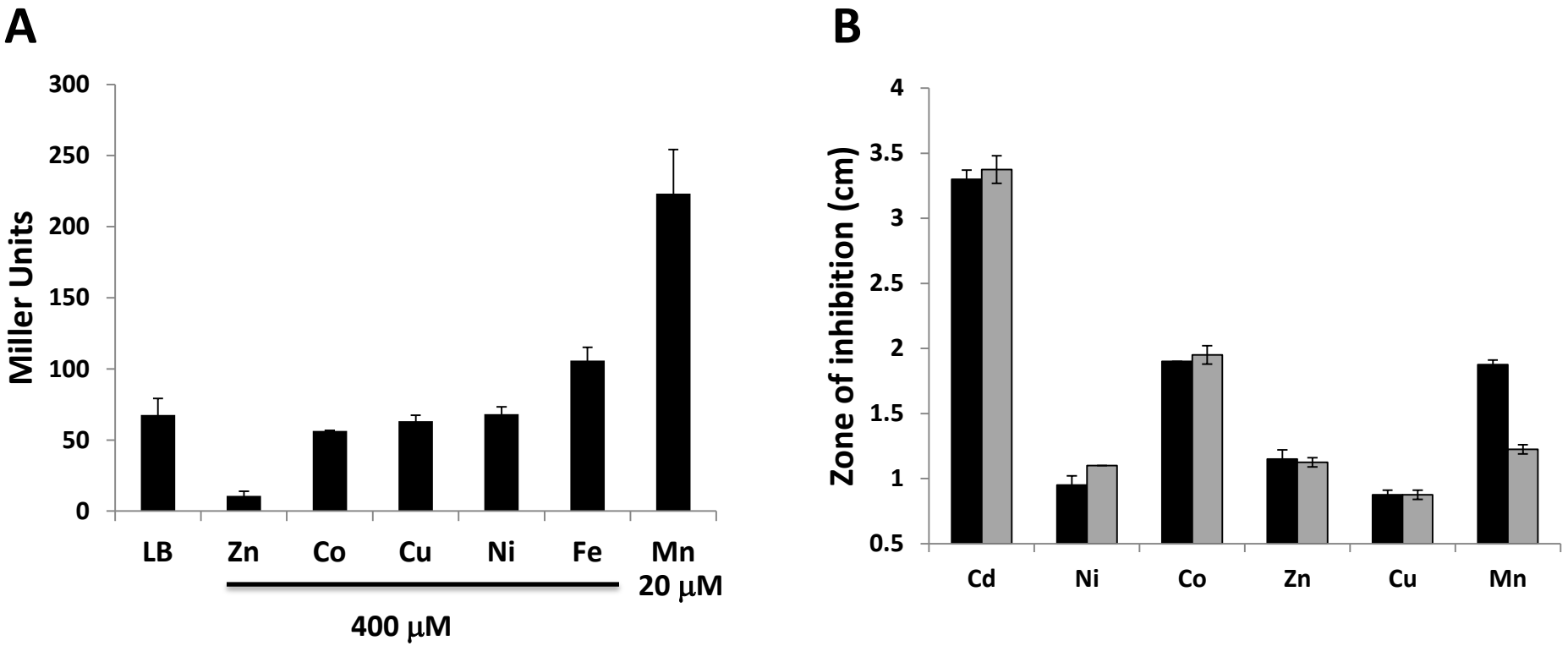
A
Miller Units
300
250
200
150
100
50
0
LB
Zn
Co
Cu
Ni
Fe
Mn
20 μM
400 μM
B
Zone of inhibition (cm)
4
3.5
3
2.5
2
1.5
1
0.5
Cd
Ni
Co
Zn
Cu
Mn

Supplemental Figure Legends

Figure S1, Experimental electron density of the Mn^{2+}-bound *L. lactis yybP-ykoY* riboswitch structure, related to Figure 2. A) Overall 2Fo-Fc electron density, contoured at 2.5 σ level. The structure model is colored according to the secondary structure model in Figure 2. B) Sequence conservation in the *L. lactis yybP*-ykoY mapped on the 3D crystal structure. Residues over 96% conserved are colored in red, over 92% in orange, as reported by Rfam. These residues cluster around the docking interface, where two highly coordinated metal ions bind. C) 2Fo-Fc electron density for the M_B site and M_A site in the 100 μM Mn^{2+} structure, contoured at 4 σ level. The metal-to-ligand distances (black dashed lines) and the A41 N6—U39 phoshoryl oxygen hydrogen bond (purple dashed line) are labeled. D) Close-up view of the cross-helix Type I A-minor motif interaction between A9 of L1 and C37-G60 of L3 in the *L. lactis* Mn^{2+}-bound structure.

Figure S2, Ba^{2+} and Mn^{2+} sites revealed by the anomalous data collection in the *L. lactis yybP-ykoY* structure, related to Figure 2. in the presence of 2.5 mM Mn^{2+}. A) The anomalous difference peaks (7 σ contour level) at the Mn K-edge are shown in teal. Due to strong anomalous absorption of Ba at the Mn K-edge, these peaks could correspond to either Ba^{2+} or Mn^{2+}. The anomalous difference map far below the Mn K-edge (6 σ contour level) is shown in red, these peaks correspond to Ba^{2+} only. Metal identities were assigned based on this criteria as well as the metal-ligand distances, the assigned Ba^{2+} ions are shown in black, Mn^{2+} in magenta, and Mg^{2+} in yellow. Note the absence of Ba anomalous signal at M_A and M_B, suggesting that only Mn occupy these sites. B) The anomalous difference map was calculated from diffraction data collected at peak of the Mn K-edge, and contoured at 9.5 σ. Mn^{2+} occupies both sites at 2.5 mM concentration.

Figure S3, Conformation and metal-binding scheme in the *L. lactis* A40U mutant structure, related to Figure 3. A) Conformation differences in the Mn^{2+} sensing L3 loop between the two monomers in the asymmetric unit of the *L. lactis* A40U mutant structure. While the two monomers are similar in overall structure, the A42 residue in the L3 loop is stacked in monomer a (in orange), but flipped out in monomer b (in cyan). B) Anomalous difference map for the A40U mutant structure, collected at the Sr absorption edge, confirming Sr^{2+} presence (at 7.5 σ). Mn contributes very little to anomalous scattering at this energy.

Figure S4, Differences between the two monomers in the asymmetric unit of the Mn^{2+}-free *E. coli yybP-ykoY* riboswitch structure, related to Figure 4. Molecule B (gray), shown in other figures, is stabilized by crystal contacts, particularly at L3. Molecule A (colored by temperature B-factors, with blue being low and red being highly flexible) displays marked flexibility around P2, P4 and the L3 loop. P2 and P4 could not be completely placed in the electron density. Both *E. coli* apo molecules differ from the *L. lactis* structure in their L1-L3 docking regions.

Figure S5, Gene context and organization of selected genes with upstream *yybP-ykoY* family riboswitches, related to Figure 5. Searching using the key words yybP-ykoY yielded 240 hits that can categorized into three groups. A) Genes encoding a putative P-type ATPase type IIA. B) *TerC* homolog *YkoY*. C) *YybP* and homologs. Few examples from each group were selected. The riboswitch aptamer is represented by a yellow box and putative terminators is represented by red circle and attenuators are represented by yellow and green circles. Analysis was done using Gene Context tool III (http://operons.ibt.unam.mx/gct3/index.jsp).

Figure S6, Architectural similarity between the hairpin ribozyme and the *L. lactis yybP-ykoY* riboswitch, related to Figure 6. Both RNAs contain a four-way-junction (cyan) and a distal cross-helix tertiary contact (light purple), mediated in part by a base flip-out (red). Major differences exist in the topology of strand cross-over at the four-way-junction, and a more extensive distal contact involving two dehydrated metal ions in the *yybP-ykoY* structure.

Figure S7, *In vivo* confirmation of *yybP-ykoY* and YoaB metal selectivity, related to Figure 1F. A) Induction of beta-galactosidase from an *L. lactis* yoaB leader region-lacZ fusion in a *B. subtilis mntR* mutant strain as monitored 60 min. after addition of various metals to the indicated concentrations. B) Sensitivity to various metals was monitored using a disk-diffusion (zone-of-inhibition) assay in the *B. subtilis mntR* Mn^{2+}-sensitive mutant (gray) and *mntR* P_{spac}-*yoaB*, which expresses *L. lactis* YoaB. Only Mn^{2+} sensitivity was rescued by YoaB.

Table S1. Sequences of the RNA constructs and DNA oligonucleotides used in this study.

IVT-Llac-WT	gcgtcagcattgatttatattacgaagaatattcgggattgtatttaaaatcaaagcgctttttagatc aaatggaaagcatgaaacacttatgggtgaaaacaaaagttgacatttggtccatctttttatatg atcatttACAAAGGGGAGTAGCGTCGGTAAGACCGAAACAAAGTCGT CAATTCGTGAGATTCTCACCGGCTTTGTTGACATACTTATGTATGT TTAGCAAGACCTTTGCCAGTTTTGATATCTGGCAGAGGTCTTTTTT TGTAAAACCTCTCATGATATCAGTTAGAAATAAAGGAGAATCATTA TG
IVT-Llac-A40U	gcgtcagcattgatttatattacgaagaatattcgggattgtatttaaaatcaaagcgctttttagatc aaatggaaagcatgaaacacttatgggtgaaaacaaaagttgacatttggtccatctttttatatg atcatttACAAAGGGGAGTAGCGTCGGTAAGACCGAAACAAAGTCGT CTATTCGTGAGATTCTCACCGGCTTTGTTGACATACTTATGTATGT TTAGCAAGACCTTTGCCAGTTTTGATATCTGGCAGAGGTCTTTTTT TGTAAAACCTCTCATGATATCAGTTAGAAATAAAGGAGAATCATTA TG
IVT-Llac-A40G	gcgtcagcattgatttatattacgaagaatattcgggattgtatttaaaatcaaagcgctttttagatc aaatggaaagcatgaaacacttatgggtgaaaacaaaagttgacatttggtccatctttttatatg atcatttACAAAGGGGAGTAGCGTCGGTAAGACCGAAACAAAGTCGT CGATTCGTGAGATTCTCACCGGCTTTGTTGACATACTTATGTATGT TTAGCAAGACCTTTGCCAGTTTTGATATCTGGCAGAGGTCTTTTTT TGTAAAACCTCTCATGATATCAGTTAGAAATAAAGGAGAATCATTA TG
SHAPE-Llac-wt	ATAAGAATTCTAATACGACTCACTATAGGCCTTCGGGCCAACAAA GGGGAGTAGCGTCGGTAAGACCGAAACAAAGTCGTCAATTCGTG AGATTCTCACCGGCTTTGTTGACATACTTATGTATGTTTAGCAAGA CCTTTGCCGATCCGGTTCGCCGGATCCAAATCGGGCTTCGGUCC GGTTC
Llac-ykoy-cryst-1	TTAAAgaattcTAATACGACTCACTATAGAAAGGGGAGTAGCGTCGG GAAACCGAAACAAAGTCGTCAATTCGTGAGGAAACTCACCGGCTT TGTTGACATACGAAAGTATGTTTAGCAAGACCTTTCCGGGCGGCA TGGTCCCAGCCTCCTGCTGGCGCCGCCTGGGCAACATTCCGAG GGGACCGTCCCCTCGGTAATGGCGAATGGGACCggatcc
Eco-ykoy-cryst-1	TTAAAgaattcTAATACGACTCACTATAGGATTTGGGGAGTAGCCGA TTTCCGAAAGGAAATGTACGTGTCAACATACTCGTTGAAAAACGT GGCACGTACGGACTGAAGAAATTCAGTCAGGCGAGACCATATCC GGGCGGCATGGTCCCAGCCTCCTGCTGGCGCCGCCTGGGCAAC ATTCCGAGGGGACCGTCCCCTCGGTAATGGCGAATGGGACCggat cc
Llac-cryst-A40U	TTAAAgaattcTAATACGACTCACTATAGAAAGGGGAGTAGCGTCGG GAAACCGAAACAAAGTCGTCTATTCGTGAGGAAACTCACCGGCTT TGTTGACATACGAAAGTATGTTTAGCAAGACCTTTCCGGGCGGCA TGGTCCCAGCCTCCTGCTGGCGCCGCCTGGGCAACATTCCGAG GGGACCGTCCCCTCGGTAATGGCGAATGGGACCggatcc
Lactis yoaB-R	GCGagatcTTAATGTTTTTCAAAAACGCCTTTA
Lactis yoaB-F	CGCaagcTTAGAAATAAAGGAGAATCATTATG
Lactis Mn ribo-lacZ-F	GCGaagctTCGAGAAGCTATTAAATTTATTAGA
Lactis Mn ribo-lacZ-R	CGCggaTCCTCTAAAACTTCATTGACGGA